VII International Conference on Particle-Based Methods
PARTICLES 2021
P. Wriggers, M. Bischoff, E. Oñate, A. Düster & T. Zohdi (Eds)

MICROMECHANICAL FRAMEWORK FOR A 3D SOLID COHESION MODEL –IMPLEMENTATION, VALIDATION AND PERSPECTIVES

MOHAMMAD SANAYEI[*], ABBAS FARHAT[†], LI-HUA LUU[†], LUKAS WERNER[‡], CHRISTOPH RETTINGER[‡], PIERRE PHILIPPE[†] AND PABLO CUÉLLAR[*]

[*] Federal Institute for Materials Research and Testing (BAM)
Division 7.2 for Buildings and Structures
Unter den Eichen 87, 12205 Berlin, Germany
e-mail: mohammad.sanayei@bam.de; http://www.bam.de/

[†] RECOVER, INRAE Aix Marseille Univ
3275 route Cézanne, 13100 Aix-en-Provence, France
email: pierre.philippe@inrae.fr, https://www.inrae.fr

[‡] Friedrich-Alexander-Universität Erlangen-Nürnberg
Chair for System Simulation,
Cauerstraße 11, 91058 Erlangen, Germany
https://www.cs10.tf.fau.de

Key words: Granular Cohesive Materials, DEM, Micromechanical Tensile Failure, Macromechanical Sample Strength.

Abstract. This article presents a solid cohesion model for the simulation of bonded granular assemblies in the frame of 3D discrete element approaches (DEM). A simple viscoplastic cohesion model for 2D geometries is extended to 3D conditions, while its yield criterion is generalized as a hyper-surface in the space of bond solicitations to include torsional moments. The model is then calibrated using experimental results of uniaxial traction at both the microscopic and macroscopic scales with an artificial granular cohesive soil. The paper finally presents some simulated results on the macromechanical sample traction application and briefly discusses the model's current limitations and promising prospects for subsequent works.

1 INTRODUCTION

Natural soil deposits such as carbonate sands in the marine environment may show an effective cohesion due to intergranular solid bridges formed by calcareous precipitation. Such cementation effect endows the granular material with the ability to resist some degree of tensile stress in addition to the compressive and shearing resistance proper of uncemented frictional sands [1]. The tensile resistance of such materials may be quantified based on measures of debonding force at the micro-scale and using appropriate homogenization techniques [2]. However, it is still a challenge to assess the influence of solid intergranular cohesion on the mechanical behaviour of soils in many practical engineering problems (e.g. on the erodibility of soils [3,4]). Recent advances both in computational hardware and parallelization strategies

make it nowadays possible to address such problems from a micromechanical perspective [5].

Here we introduce a simple model for solid cohesion and its implementation within a 3D discrete element framework. The model involves a classical viscoelastic bond rheology and specific debonding modes for tensile, shearing, bending and torsional solicitations.

We finally present a calibration of the model to match experimental data from an artificial granular soil made out of cemented glass beads [2] and a validation of the approach with a macro-mechanical application.

2 SOLID GRANULAR MECHANICS

As basic computational framework we use here a purely frictional DEM scheme in 3D [6], which is complemented by a simple viscoplastic cohesion model [2,5,7] that has now been extended to 3D conditions and also takes torsional interactions into account..

2.1 Frictional DEM

A 3D rigid particle dynamics method based on Newton's second law of motion is used to describe the interactions between particles. The frictional interactions are formulated in terms of the normal force, and the three different tangential forces and torque laws (see also [6]): (i) Coulomb's friction, (ii) rolling resistance and (iii) torsion resistance. The normal force, F_n, depends on the local overlap between two particles, δ_n, the normal stiffness, k_n, and the damping coefficient η_n. The shear force is calculated incrementally using the relative sliding velocity, V_s, with the friction stiffness K_s , and the frictional damping η_s. The interaction torques are defined by shear force with corrected radius relative to the contact point, and, finally, the rolling and torsion resistances, f_r and f_o, are defined by the rolling velocity and the relative spin along with the particles normal direction, V_r and V_o, and quasi-forces calculated in analogy to the shear force using an incremental algorithm [6].

2.2 Cohesive bond model in 3D

For this study we have introduced a 3D extension of our previous cohesion framework for two-dimensional granular samples with solid bridges [7]. The visco-elastoplastic solid bond rheology, which was originally characterized by a set of normal, shear and bending stiffnesses, damping coefficients and yield thresholds, is now extended to 3D conditions including a further resistance and failure mode for torsional solicitations.

For the case of polydisperse couples, any bonds between particles with different radii are considered as "bars" with non-uniform cross-sections. The equivalent stiffnesses of such non-uniform bonds are calculated here using the work of [8], where k_n^b is the normal stiffness of the bond connecting particle *i* and particle *j,* and k_n is the usual normal stiffness for monodisperse contacts:

$$k_n^b = 4k_n \frac{r_i r_j}{r_i + r_j}$$

The yield criterion (Fig 1), which firstly was proposed with a paraboloidal shape by Delenne and co-workers based on experimental results [9] is now straightforwardly extended to include the torsional moment and its threshold:

$$g_u(f_n, f_s, M_r, M_o) = \left(\frac{f_n}{C_n}\right) + \left(\frac{f_s}{C_s}\right)^2 + \left(\frac{M_r}{C_r}\right)^2 + \left(\frac{M_o}{C_o}\right)^2 - 1 \quad (1)$$

where f_n and f_s are the normal and tangential forces, M_r and M_o are the rolling and torsional moments, C_n, C_s, C_r, C_o are the normal, tangential, rolling and torsion thresholds (see [6,7]), and g_u stands for the failure condition. Whenever $g_u \geq 0$, the bond between two given particles is considered as broken and any further interactions of this particle pair becomes purely frictional. For this study we have fixed the aspect ratios of the failure hyper-surface (now it involves four dimensions in the space of interactions) for different degrees of cohesion and related all bond thresholds to one single parameter C that accounts for the strength of the solid bond: $C = C_n = 2C_s = C_r / (2d\_mean) = C_o / (2d\_mean)$.

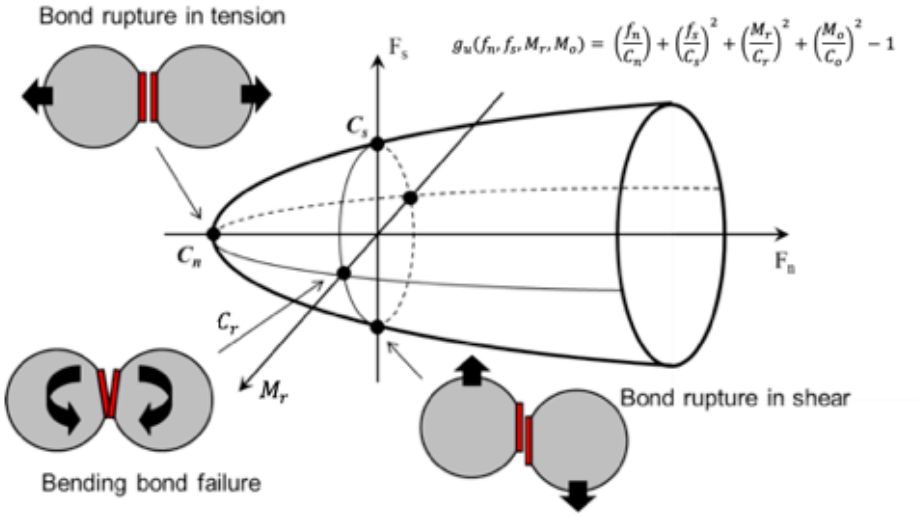

Figure 1: Original yield surface of cohesive bonds in the space of interactions, redrawn from [9]. For visual simplicity, the fourth dimension (torsional interactions) involved in the presented 3D model has been omitted in this depiction.

2.3 Implementation strategy in C++

The corresponding algorithms have been implemented at first for sequential execution using C++ programming language. The data structure for the cohesion model is initialized by considering any initial contact (overlap) between pairs of particles as a solid cohesive bridge. To have fast access to each bond specifications, all the bond properties are stored in key-value pair with unique keys data structure (balanced binary tree). This data structure is optimized for lookups with the cost of log(N) time complexity, where N is the number of particles inside the model (see [10]). During the simulation, if the cohesion bond between a pair of particles is broken, the bond information will be deleted, and the interaction between them will be treated as purely frictional from that step.

In each time step, after investigating the interactions between all particles and walls, the particles' kinematics is updated using a Velocity Verlet algorithm [11]. In this implementation, the most time-consuming part of calculation is the detection and treatment of interactions between two particles or between particles and the walls inside a nested for loop because of

having quadratic time complexity. For our subsequent studies, this approach will be replaced with an algorithm like linked cell (see [5]), which is a cell-based algorithm for keeping the track of particles entering each neighbor cell. This way, each particle will be assigned to a particular spatial cell and updated with a given frequency. This assignment has a linear time complexity and after that, only particles in neighboring cells will be investigated for overlapping, which reduces considerably the computational cost of the neighbor detection. Also, with the development of multi-core CPUs, fork-join models (OpenMP) can be used for nested loops parallelization.

3 EXPERIMENTAL CHARACTERIZATION

We employ here some experimental data from an artificial granular soil made out of cemented glass beads to calibrate the presented cohesion model. This cohesive material is composed of spherical borosilicate beads with uniform diameter d bonded by solidified paraffin capillary bridges with a mass content of x_p (see further details in [2]).

3.1 Single-bond tensile threshold

The tensile strength of a single paraffin solid bond has been measured with the experimental setup illustrated in Fig.2-left, where a bonded couple of beads is placed vertically, the upper bead being connected to a scale through a clamp and a soft spring while the lower one being fixed to a slowly receding bottom plate. The micro-tensile force at failure F_m (which would correspond to the normal yield threshold C_n of the cohesion model above) is then measured as the mass increment ($\Delta m = m_{peak} - m_{residual}$) times gravity ($g = 9.81$ m/s^2). The results for different particle sizes and different paraffin contents is summarized in the right pane of Fig. 2, where the corresponding data for the 4mm beads and 1% paraffin mass (to be used later on for the simulations) features an average value of $F_{m,av}$=421 mN, with a standard deviation of 225 mN.

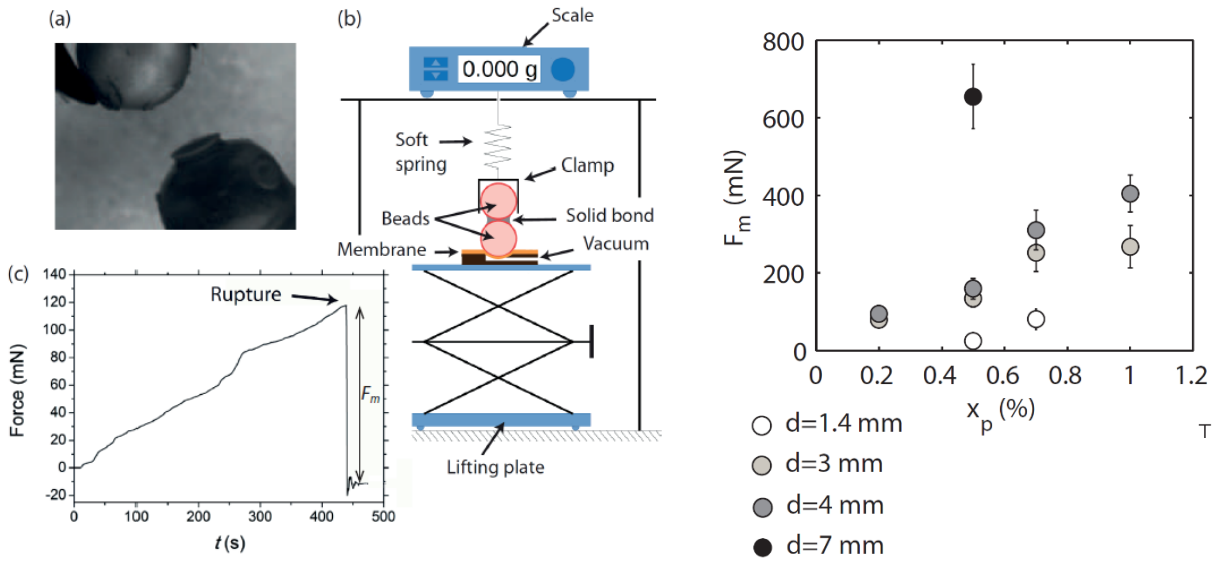

Figure 2: Single-bond tensile tests. Left: (a) Broken paraffin solid bridge between two glass beads (d=4 mm and x_p=1%). (b) Setup for the single-bond tensile test. (c) Typical evolution of the force measured during the test, with the resulting bond tensile strength at failure F_m. Right: Measured threshold F_m for different particle sizes d and paraffin contents x_p. Sources: [2]

3.2 Cohesive strength of granular sample

A measure of the global cohesion strength of the material was obtained at a macro-scale with traction tests involving an "hourglass cell" with two detachable conical parts (see left panel of Fig.3). The test cells were manufactured in three different sizes (with respective neck diameters of D=30mm, 56mm and 79 mm) in order to investigate potential boundary effects while keeping a similar aspect ratio. The bonded granular samples were then prepared and solidified directly within the assembled cell. The traction tests were finally conducted by lifting the mobile platform at a constant velocity (0.1 mm/min for the small and medium devices, and 0.3 mm/min for the large device) until separation of the two cones. The macroscopic cohesive strength of the sample σ_M is thereby measured in terms of the recorded force at rupture, F_M, divided by the failure section, i.e. $\sigma_M = F_M/((\pi/4)\cdot D^2)$. The results for the different test devices, particle sizes, and paraffin contents are summarized in the right panel of Fig. 3. No formal measurement has been performed by now for the specific case to be simulated here in the following section (i.e. for d=4mm and x_p=1% in the small device), but the expected average value from preliminary investigations is around 30 kPa with a substantial standard deviation as inferred from the data already obtained.

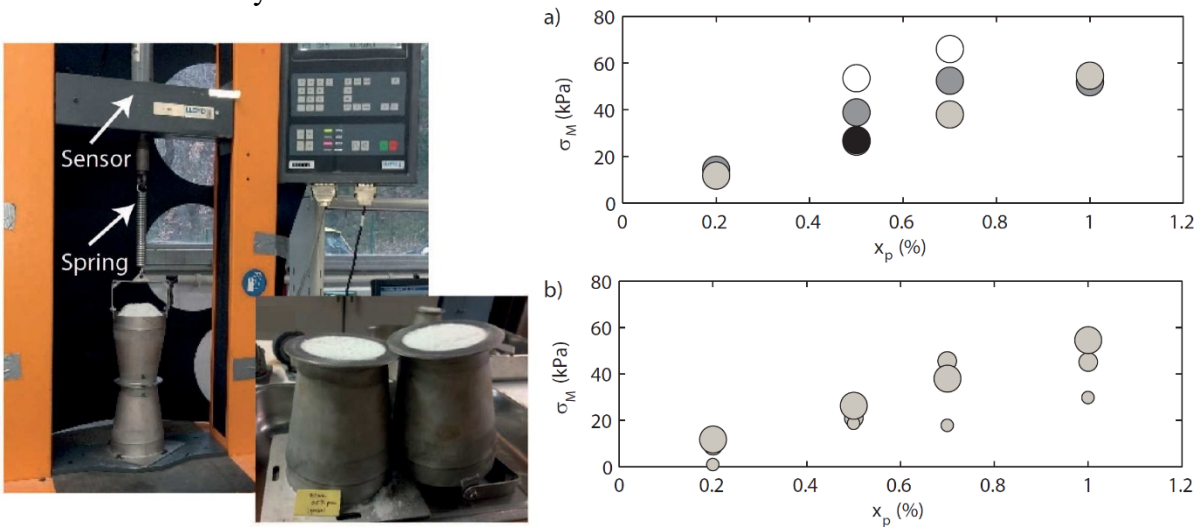

Figure 3: Cohesive sample tensile tests. Left: Pictures of the traction bench and typical failure surfaces after a test. Right: Measured sample tensile strength σ_M for different sample sizes, particle sizes d and paraffin content xp. (a) Large device with d=1.4 mm (white), d=3 mm (grey), d=4 mm (dark grey), and d=7 mm (black). (b) Large, medium and small devices (symbol size) with d=3 mm. Source: [2]

4 TENSILE FRACTURE OF COHESIVE SAMPLES

4.1 Case geometry and prescriptions. Material parameters

To create the cohesive granular sample for the sample traction test, the geometry of the small hourglass conical device is implemented inside the developed numerical model. Since the tests have shown that the majority of the bond breakages takes place around the neck of the device, and in order to reduce the computational expense, in this study only the relevant part of the

geometry in the vicinities of the device's neck is simulated (in total, just the half of the real device's height). The numerical sample is created by pouring over a thousand spherical particles with diameters ranging from 3.2 mm to 4.8 mm into the conical walls until they settle and show a negligible kinetic energy (see Fig 4a). For the initial deposition of the particles, the cohesion model is deactivated and only frictional contacts between particles are considered. For the tensile test simulation, the settled geometry is adopted as initial configuration and the cohesion model is activated, whereby all particle couples with an initial overlap are considered as bonded pairs with a cohesive strength corresponding to the average micromechanical strength of solidified paraffin capillary bridges with a mass content of xp= 1%.

As boundary conditions for the test, all particles in contact to the lower conical wall are held fixed and not allowed to rotate, while the particles in contact to the upper conical section of the device are pulled upwards with a prescribed constant velocity. The rest of the particles are all considered bonded at their initial contact points but otherwise allowed to move freely (see Fig 4a). This approach permits to disregard the contact detection and interactions with conical walls, thus reducing considerably the computational cost. The simulation is then conducted until the upper cone is displaced for 1 mm and the sample is fully broken at the device's neck (Fig 4b). The geometry, material and model parameters used for this problem are summarized in Table 1.

Table 1: Geometrical, material, and model parameters

Particle mean size, d_{mean}	4×10^{-3} m
Polydispersity, d_{max}/d_{min}	1.5
Cone height, h	0.081 m
Hourglass neck diameter, D	0.030 m
Cone base diameter, D_b	0.040 m
Particle density, ρ_s	$2600\ kg/m^3$
Normal contact stiffness, k_n	$5.1 \times 10^7\ N/m$
Shear contact stiffness, k_s	$5.1 \times 10^7\ N/m$
Rolling stiffness, k_r	$0.1\times k_n$
Torsion stiffness, k_o	$0.1\times k_n$
Friction coefficient, μ	0.3
Bond Strength, C	$0.42\ N$
Time step, dt	$5.6 \times 10^{-6} s$

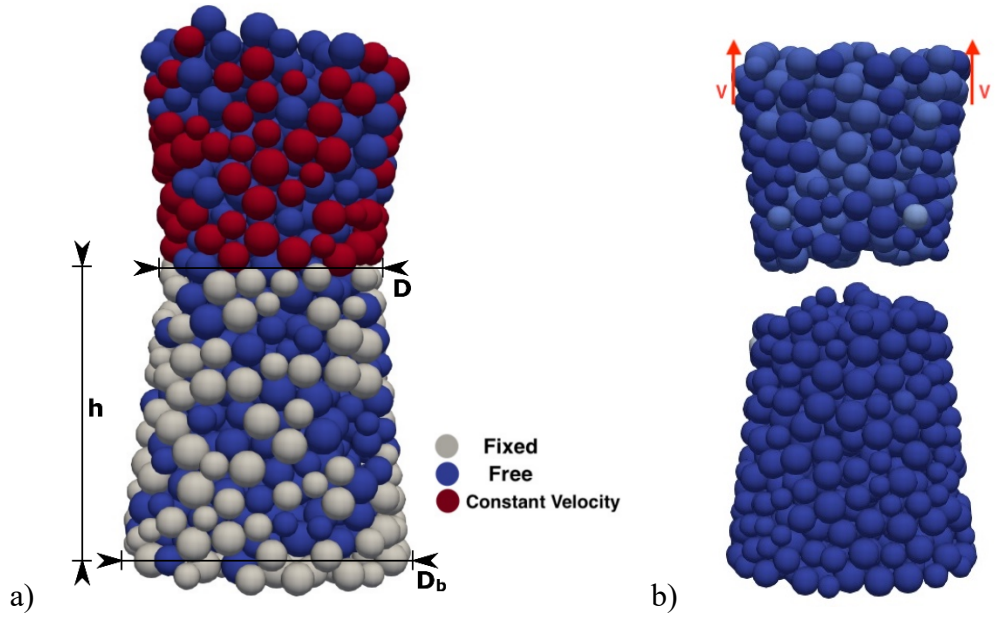

Figure 4: Geometry and boundary conditions of the cohesive sample traction problem. a) Initial sample state and prescriptions, where white particles are fixed, red particles have a prescribed constant velocity *v* (upwards vertical) and the blue particles are initially bonded but have no other kinematic constraints; b) Exemplary sample state after failure with a constant pull-up rate v

4.2 Numerical results and discussion

The sum of the reaction forces acting on the grains with prescribed velocity (red particles in Fig.4) plus their own weight, yields the magnitude of the force F_z required for separating the upper cone from the lower cone and eventually to the sample's cohesive strength at failure (difference between the peak and residual values of the pulling force F_z). The evolution of the simulated pulling force for three different pull-up rates is shown in Fig.5, where the sample is characterized by a relatively brittle failure within the first few microns of sample elongation.

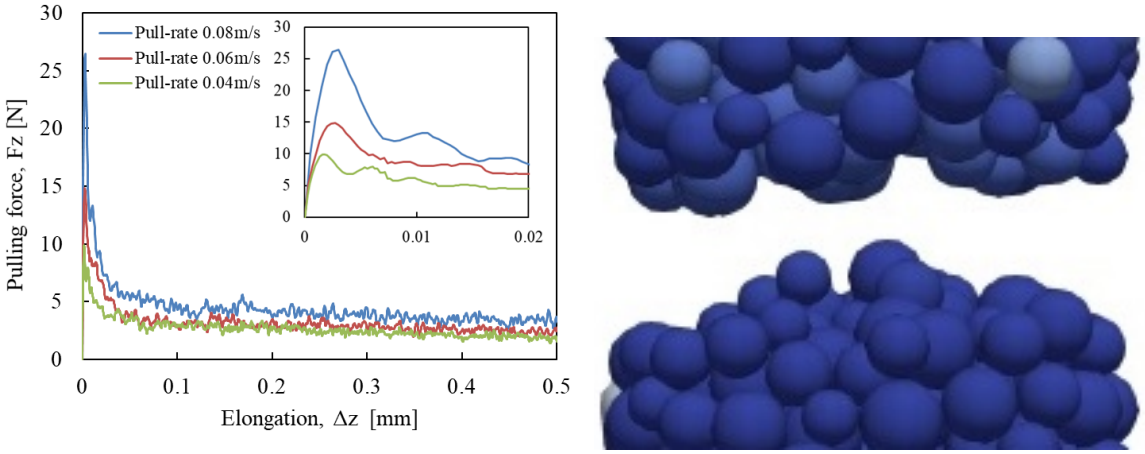

Figure 5: Simulated sample traction test. Left: Tensile force for different pull-up rates. Right: Final shape of the sample failure surface.

The macro-mechanical sample strength shows a strong dependency on the pulling rate despite all viscous parameters of the cohesion model being explicitly set to zero, which appears to indicate that the inherent dynamic character of the DEM approach plays a dominant role in this particular case.

A first comparison to the experimental test results shown in section 3 above indicates a fair agreement on the macroscopic sample strength, with simulated values of σ_M up to 35kPa, which lies in the right order of magnitude for the average sample strength and well within the measured ranges [2].

Figure 6 finally provides an insight into the micromechanics of the sample, where the bond normal forces are depicted shortly before and after failure, showing the expected stress concentration at the sample's neck.

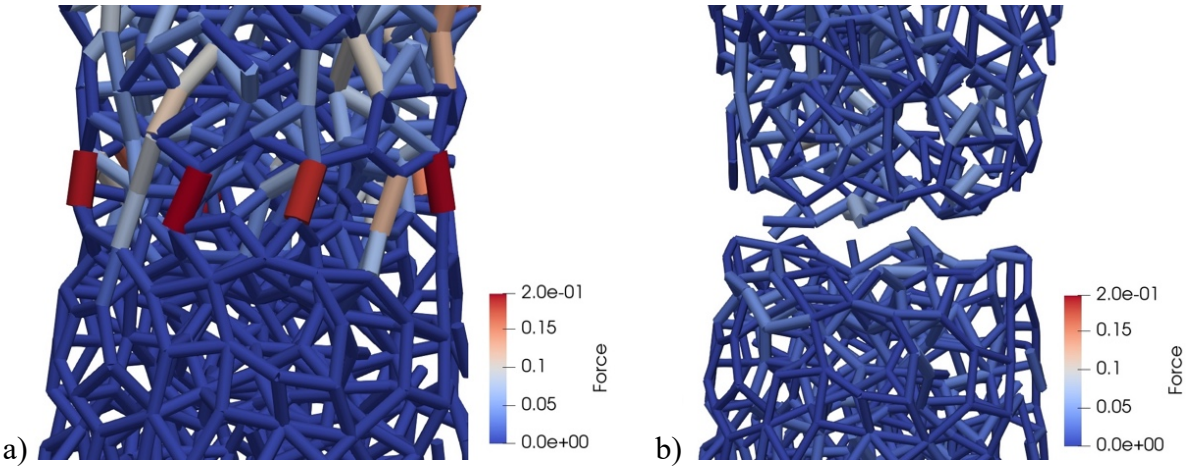

Figure 6: Normal forces in the cohesive bonds, a) shortly before failure, where mainly the bonds around the cone neck are activated, b) and stress relaxation at both sides of the broken neck after sample failure.

5 CONCLUSIONS AND OUTLOOK

The micromechanical tensile threshold of the presented 3D model for solid cohesion has been calibrated with experimental data from single-bond traction tests, while the rest of material parameters have been preliminary adopted from arbitrary sets of values and relationships from the literature. The preliminary macro-mechanical simulations show already a fair agreement with the experimental sample strength. However, the strong dependency on the pulling rate and the wide range of possible material behaviors based on the single choices for the tensile threshold and stiffness parameters, from an elastic "chain-like" behavior with progressive debonding to stiff brittle behavior, call for a detailed parametric analysis and a proper calibration process involving a back-analysis of the macroscopic experimental data.

In the next steps of this study, the linked cell algorithm will be introduced to the numerical model for tracking particles in each neighboring cell, to increase the model efficiency for overlap detection. Furthermore, the contact detection between two particles and wall-particle can be performed independently so that the fork-join model (OpenMP) will be used for loop parallelization.

However, in order to profit from a robust and optimized HPC (high performance computing), this cohesion model can also be integrated into the open-source framework waLBerla [12],

which is a block-structured high-performance platform for multiphysics simulations that includes efficient algorithms for both the DEM and Lattice Boltzmann techniques among others. Using this framework, complex geometries can be efficiently divided into block-structured grids which makes it flexible for running the simulation on CPU- and GPU- clusters. So far, the mechanics of the cohesion bond model have already been implemented into this platform and are now undergoing the subsequent stages of validation and performance optimization.

Finally, the cohesion model implemented in this study is appropriate to reproduce the cohesive response of bonded grains under either quasi-static or fully dynamic impacts. However, this model cannot reproduce the progressive degradation of single bonds because it lacks the transitional stages of the bond between the intact and the completely broken states. So, in future studies, following the work of [13], the damage model for bonded particles will be introduced.

ACKNOWLEDGEMENTS

This work is part of the COMET research project, funded by the Deutsche Forschungsgemeinschaft (DFG grant number 406907912, project ID: CU 393/1-1) and the French Agence Nationale de la Recherche (ANR; grant number ANR-2018-CE92-0007), whose support is gratefully acknowledged. Fruitful discussions and kind support have been provided by Vincent Richefeu.

REFERENCES

[1] Collins, B.D. and Sitar, N., (2009). Geotechnical Properties of Cemented Sands in Steep Slopes. *Journal of Geotechnical and Geoenvironmental Engineering*, **135**(10): 1359-1366.

[2] Farhat, A., Luu, L. H., Philippe, P., & Cuéllar, P. (2021). Multi-scale cohesion force measurements for cemented granular materials. In *EPJ Web of Conferences* (Vol. 249, p. 08008). EDP Sciences.

[3] Brunier-Coulin, F.; Cuéllar, P. and Philippe, P. (2020). Generalized Shields criterion for weakly cohesive granular materials, *Physical Review Fluids*, **5**(3), 034308.

[4] Philippe, P., Benseghier, Z., Brunier-Coulin, F., Luu, L. H., Cuéllar, P., & Bonelli, S. (2021). Extending the Shields criterion to erosion of weakly cemented granular soils. In *EPJ Web of Conferences* (Vol. 249, p. 08009). EDP Sciences.

[5] Benseghier, Z.; Cuéllar, P.; Luu, L.-H.; Bonelli, S. and Philippe, P. (2020). A parallel GPU-based computational framework for the micromechanical analysis of geotechnical and erosion problems. *Comput. Geotechn*. **120**, 103404

[6] Luding, Stefan. "Introduction to discrete element methods: basic of contact force models and how to perform the micro-macro transition to continuum theory." *European journal of environmental and civil engineering* 12.7-8 (2008): 785-826.

[7] Cuéllar, Pablo, et al. "Numerical insight into the micromechanics of jet erosion of a cohesive granular material." *EPJ Web of Conferences*. Vol. 140. EDP Sciences, 2017.

[8] Rojek, Jerzy, et al. "Comparative study of different discrete element models and evaluation of equivalent micromechanical parameters." *International Journal of Solids and*

Structures 49.13 (2012): 1497-1517.

[9] Delenne, Jean-Yves, et al. "Mechanical behaviour and failure of cohesive granular materials." *International Journal for Numerical and Analytical Methods in Geomechanics* 28.15 (2004): 1577-1594.

[10] Stroustrup, Bjarne. The C++ programming language. Pearson Education, 2013.

[11] Holm, Christian. "Simulation Methods in Physics." Institute for Computational Physics. University of Stuttgart 2013 (2012)

[12] Bauer, M.; Eibl, S.; Godenschwager, C.; Kohl, N.; Kuron, M.; Rettinger, C.; *et al*. (2020): WALBERLA: A block-structured high-performance framework for multiphysics simulations. *Computers & Mathematics with Applications* **81***: 478-501*

[13] Silvani, C., Désoyer, T., & Bonelli, S. (2009). Discrete modelling of time-dependent rockfill behaviour. *International Journal for Numerical and Analytical Methods in Geomechanics*, 33, 665-685.